energies

MDPI

Article

Synergistic Effects in Co-Gasification of Willow and Cedar Blended Char in CO_2 Media

Kenji Koido [1,2,3,*], Kenji Endo [4], Hidetsugu Morimoto [5], Hironori Ohashi [2,3] and Michio Sato [2]

[1] Department of Wood Properties and Processing, Forestry and Forest Products Research Institute, 1 Matsunosato, Tsukuba 305-8687, Japan
[2] Faculty of Symbiotic Systems Science, Fukushima University, 1 Kanayagawa, Fukushima 960-1296, Japan; h-ohashi@sss.fukushima-u.ac.jp (H.O.); msato@sss.fukushima-u.ac.jp (M.S.)
[3] Hydrogen Energy Research Institute, Faculty of Symbiotic Systems Science, Fukushima University, 1 Kanayagawa, Fukushima 960-1296, Japan
[4] Graduate School of Symbiotic Systems Science and Technology, Fukushima University, 1 Kanayagawa, Fukushima 960-1296, Japan; ohb3260330z295v@gmail.com
[5] Graduate School of Bioresources, Mie University, 1577 Kurimamachiya-cho, Tsu 514-8507, Japan; morimoto@bio.mie-u.ac.jp
* Correspondence: koido@ffpri.affrc.go.jp; Tel.: +81-29-829-8305

Abstract: Willow is a promising biomass resource for addressing the challenges of securing stable domestic biomass fuels in Japan and utilising abandoned agricultural land. Among the willow species, *Salix pet-susu Kimura KKD* (known as ezonokinu willow, EW) stands out for its growth, high production, storage stability, production stability, and business stability. Previous studies have investigated fuel characterisation through gasification (co-gasification) of various biomass mixtures to enhance feedstock flexibility for gasifier commercialisation. However, the synergistic effects of co-gasification using fuels containing EW blended with Japanese cedar, a commonly planted forest species in Japan, remain unexplored. Therefore, this study explored CO_2 co-gasification with different blend ratios of EW/cedar blended char and evaluated the fuel characteristics for each blend ratio to elucidate the synergistic effects. The prepared char samples were utilised in the CO_2 gasification test with TG-DTA as the analyser. The results suggest that in the initial stages of the willow/cedar blended char co-gasification reaction, pore size and specific surface area significantly influence the reaction rate. Subsequent stages of the reaction are influenced by the promoting and inhibiting effects of inorganic components, which impact co-gasification. The synergy factor results for the willow/cedar blended char co-gasification suggest a reaction pathway.

Keywords: char co-gasification; CO_2 diffusion in char; synergistic effect; reactivity; willow; reaction pathway

Citation: Koido, K.; Endo, K.; Morimoto, H.; Ohashi, H.; Sato, M. Synergistic Effects in Co-Gasification of Willow and Cedar Blended Char in CO_2 Media. *Energies* **2024**, *17*, 4122. https://doi.org/10.3390/en17164122

Academic Editors: Jakub Mularski and Halina Pawlak-Kruczek

Received: 15 July 2024
Revised: 6 August 2024
Accepted: 11 August 2024
Published: 19 August 2024

1. Introduction

The Paris Agreement, adopted in 2015, set a long-term goal of limiting global average temperature rise well below 2 °C above pre-industrial levels, with efforts to limit it to 1.5 °C. Accordingly, in 2020, Japan announced its plan to eliminate domestic greenhouse gas (GHG) emissions and be "carbon neutral by 2050". Additionally, at the 2021 Climate Summit, Japan committed to reducing GHG emissions by 46% by 2030 compared to 2013 levels. Achieving these targets necessitates a significant shift toward renewable energy sources. Given Japan's ample forest resources, integrating woody biomass with solar and wind power is anticipated.

Driven by its 2012 renewable energy feed-in tariff scheme, woody biomass power generation capacity has increased along with demand. However, large-scale steam turbine-based woody plants require significant quantities of woody fuel, leading to challenges in sustainability, including the importation of scarce biomass.

Conversely, small-scale woody biomass gasification combined with heat and power (CHP) plants can efficiently generate electricity and utilise heat at small outputs of 50–2000 kW. Given the relatively narrow resource collection area and low transport costs, this combination is expected to become a decentralised energy generation system fuelled by local forest biomass resources. CHP can convert woody biomass into thermal and electric energy. The gasification process converts woody biomass into producer gas, which is subsequently utilised by a gas engine to produce rotary power that drives the generator shaft to generate electricity. The sensible heat generated during this process can be reclaimed through heat exchange with water to produce hot water. In the gasifier, woody biomass is dried by heat and then pyrolysed, followed by a reduction reaction of the pyrolysed char. The main reaction formulae that occur in the gasifier are listed in Table 1. Considering that the drying and pyrolysis reactions and the main reduction reactions of woody fuel are endothermic, partial combustion is performed by blowing air into the pyrolysis char to compensate for the reaction heat.

Table 1. Main chemical reactions in woody biomass gasification [1–3].

Reaction		Reaction Formula	Standard Heat of Reaction [kJ/mol]	Reaction Formula Number
Pyrolysis	Pyrolysis reaction	$C_xH_yO_z \rightarrow aCO_2 + bH_2O + cCH_4 + dCO + eH_2 + fC_2 + \text{char} + \text{tar}$		(R1)
Oxidation	Combustion	$C + O_2 \rightarrow CO_2$	393.5	(R2)
	H_2 oxidation	$H_2 + 0.5O_2 \rightarrow H_2O$	242	(R3)
	Partial oxidation	$C + 0.5O_2 \rightarrow CO$	123.1	(R4)
Reductive reaction	Boudouard	$C + CO_2 \rightarrow 2CO$	−159.9	(R5)
	Water-gas	$C + H_2O_{(gas)} \rightarrow CO + H_2$	−118.5	(R6)
	Water-gas shift	$CO + H_2O_{(gas)} \rightarrow CO_2 + H_2$	40.9	(R7)
	Methanation	$CO + 3H_2 \rightarrow CH_4 + H_2O_{(gas)}$	205.2	(R8)
	Steam methane reforming	$CH_4 + H_2O_{(gas)} \rightarrow CO + 3H_2$	−206	(R9)

Specifically, two main types of gasification reactions of woody biomass fuels occur in gasifiers. The first is steam gasification (water-gas reaction (R6)), in which CO and H_2 are produced by the reaction between steam from the moisture contained in the woody biomass fuel and the pyrolysis char. The second is CO_2 gasification (Boudouard reaction (R5)), which occurs through the reaction of pyrolysis char with the CO_2 produced by the combustion of pyrolysis char (R2). The CO_2 gasification of pyrolysis char is the rate-limiting step of the process, as the reaction rate is slower than that of steam gasification and thus determines the remaining rate of char. Many studies on the CO_2 gasification of pyrolysis char have been conducted [4]. In biomass gasification, drying of the biomass occurs first, followed by a pyrolysis reaction that takes a few minutes. The reaction rate of the CO_2 gasification of char is slower than that of the steam gasification of char. Therefore, the CO_2 gasification of char is the rate-limiting step in biomass gasification. Hence, it was necessary to clarify the rate of char CO_2 gasification. The char CO_2 gasification rate is important for estimating the timing of residue discharge from the gasifier.

The kinetics of the CO_2 gasification reaction of the pyrolysis char are specified by reactivity. The reactivity of woody biomass-derived char is influenced by three main factors [5]: (i) the content and composition of inorganic elements, (ii) the physical structure, including the specific surface area and pore size distribution, and (iii) the content of functional groups and the chemical structure of the carbon matrix. Co-gasification, in which different biomass species are mixed and gasified together, has been considered as an approach to control inorganic elements (i) and the carbon matrix (iii). Co-gasification of biomass char is a synergistic process in which different char samples are combined and gasified to enhance reactivity by facilitating reactions with alkali and alkaline earth metals (AAEMs) and increasing the degree of disorder in the carbon structure [6]. AAEMs have a catalytic effect on char conversion through the oxygen transfer cycle [3,7–9].

In previous studies, co-gasification of coal and woody biomass chars was performed, and fuel characterisation was conducted. Coal and woody biomass char are often produced by pyrolysis of a mixture of pulverised coal and pulverised woody biomass [4,10–14]. In the study by Hyo Jae Jeong et al. [11] pyrolysed a mixture of Shinhwa coal and pine sawdust at mass ratios of 4:1, 1:1, and 1:4 to obtain char samples. They co-gasified each char sample with CO_2 at 900–1100 °C. A synergistic reactivity effect was observed in the biomass blended char, which increased with the amount of biomass utilised. To interpret the carbon conversion data, a random pore model (RPM) was employed to derive the reaction rate constants. Activation energy and pre-exponential coefficients were obtained for each coal/biomass mixing ratio using the Arrhenius equation.

Juntao Wei et al. [13] examined the effects of gasification temperature (900–1100 °C) and blend ratios (3:1, 1:1, 1:3) on the reactivity of petroleum coke and biomass co-gasification using TGA. The results showed that increasing the biomass proportion and gasification temperature enhanced char gasification reactivity. The synergistic effect on reactivity peaked at 1000 °C and weakened as the temperature rose to 1100 °C, which is related to molten biomass ash rich in glassy potassium and reduced inhibition of active potassium transformation above 1000 °C.

Juntao Wei et al. [14] investigated the co-gasification reactivity of rice straw and bituminous coal/anthracite blended chars under CO_2 using thermogravimetric analysis. The study quantitatively examined how coal type and gasification temperature influence synergy behaviour as carbon conversion increases. It also analysed AAEM species' chemical forms and concentrations to understand the co-gasification synergy mechanism. Results showed that for rice straw-bituminous coal blends, inhibition effects weakened first, and then synergy effects were enhanced as conversion increased. Higher temperatures prolonged the inhibition effects. For rice straw-anthracite blends, synergy effects were strong initially and weakened after peaking in the middle stage. Synergy behaviour in rice straw-bituminous coal blends was due to active K and Ca transformations, while in rice straw-anthracite blends, it correlated with active K transformation.

On the other hand, there are also cases for gasification of blended char samples of pulverised coal pyrolysis char and pulverised woody biomass pyrolysis char [15]. Hai-bin Zuo et al. [15] examined the isothermal gasification reactivity of biomass char and coal char blends (ratios 1:3, 1:1, 3:1) at 900, 950, and 1000 °C under CO_2 using thermogravimetric analysis (TGA). Increasing the biomass char ratio led to a higher gasification rate and shorter gasification time due to the biomass char's high specific surface area and coal char's uniform carbon structure. The reaction behaviour was best described by the RPM. Synergistic effects were observed at all blend ratios and increased with the gasification temperature.

However, in the case of woody biomass gasification in a fixed-bed gasifier, wood chips are gasified. Since the wood chips are not pulverised as finely as coal, each wood chip is pyrolysed separately to form char in the gasifier, and the char is then mixed and gasified. Therefore, the effect of blending chars from pyrolysing one wood species with chars from a different species on the synergistic effect and reaction rate was unclear.

Fuel characterisation has been conducted for various biomass mixtures to enhance feedstock flexibility (co-gasification) for the commercialisation of gasification systems using biomass as feedstock. Previous studies have explored the use of different combinations of agricultural residues, such as corncobs, rice husks, sesame stalks, and cotton gin refuse [16]; a mixture of woody and herbaceous wastes along with agricultural residues, including sawdust, bamboo flour, and rice husks [17]; and a combination of underutilised agricultural residues, such as coconut shells (CS) and oil palm fronds (OPF) [18,19], oil palm trunk and fronds [20], and corn and coconut residues [21]. Other studies have investigated the blending of agricultural residues or waste materials with wood, such as CS and charcoal [22], pine wood and post-extraction rapeseed meal [23], wood-coconut fibre pellets and rice husk [24], municipal solid waste and biomass [25,26], and woody biomass and chicken manure [27]. Additionally, Youjian Zhu et al. [28] conducted co-gasification experiments using

mixed fuels of aquatic cultivated biomass, large algae, microalgae, and woody biomass (Table 2). However, the co-gasification characteristics of terrestrial cultivated woody and underutilised biomass have not yet been investigated.

Table 2. Previous studies on co-gasification of blended biomass.

Feedstock	Classification	Reactor Type	Process Conditions	Product and Yield	Reference
Corncobs, rice husks, sesame stalks, and cotton gin refuse	Unused (agricultural residue)	Fixed-bed downdraft gasifier (30 kg/h, Ankur WBG-30)	T = 880–980 °C	CGE values up to 57.91% and LHV up to 4460 kJ/kg under specific blend conditions. CGE $\leq$ 57.91%, LHV $\leq$ 4460 kJ/kg	[16]
Sawdust (SD), bamboo dust (BD) Rice husk	Waste Unused (agricultural residue)	Circulating fluidised bed gasifier	T = 800–900 °C ER = 0.19–0.35	1.72 m^3/kg-dry biomass at SD + BD, T = 800 °C, ER = 0.35	[17]
Wood chips (WDC), coconut shells, oil palm fronds	Unused (wood, agricultural residue)	Fixed-bed downdraft gasifier	T = 700–900 °C	H_2: 11.70 vol% at WDC/CS blend ratio = 70/30 Catalyst: Portland cement, dolomite, and limestone	[18,19]
Algae fuels Woody biomasses	Cultivated Unused (wood)	Fluidised bed gasifier	T = 820–882 °C	Increase in CO, H_2, and CH_4 yields by 3–20, 6–31, and 9–20% at wood/algae blend ratio = 90/10	[28]
Coconut shell charcoal	Unused (wood, agricultural residue)	Fixed-bed downdraft gasifier (50 kW)	T = 700–1000 °C	Thermal treatment of gasifier-producing tar	[22]
Pine wood, Post-extraction rapeseed meal (RM)	Unused (wood, agricultural residue) Waste	Fluidised bed gasifier (4 kW)	T_1 = 800 °C (over the grate), T_2 = 450 °C (in the fuel layer), T_3 = 850 °C (over the fuel layer)	CO, H_2, CO_2, and CH_4 composition = approximately 22%, 8%, 19%, and 14% at wood/RM blend ratio = 70/30	[23]
Wood-coconut fibres pellet (WCF), rice husk (RH)	Unused (wood, agricultural residue)	Fixed-bed downdraft gasifier	T = 400–850 °C (pyrolysis zone) T = 100–1200 °C (oxidation zone)	Highest LHV of syngas (4.07 MJ/Nm^3) at RH/WCF blend ratio = 0/100 pellet with 85% efficiency	[24]
Oil palm trunk (OPT) and frond (OPF)	Unused (agricultural residue)	Fixed-bed downdraft gasifier	T = 800 °C	The highest gas constituents are CO, H_2, and CH_4 (gas yield = 1.47 Nm^3/kg and HHV = 6.85 MJ/Nm^3) at an OPT/OPF blend ratio of 30/70	[20]
Corn residues (CR) and coconut shells (CS)	Unused (agricultural residue)	Fixed-bed downdraft gasifier	T = 900 °C	Positive synergistic effect of CO, CH_4, and H_2 composition (23.81%, 11.56%, and 7.59%) at CR/CS blend ratio = 20/80	[21]
Municipal solid waste, switchgrass	Waste Cultivated	Fixed-bed downdraft gasifier (commercial scale)	T = 700–900 °C	At blend ratio = 20%/40%, CO and H_2 (12.6%/14.1%, and 8.6%/0%), with syngas LHV = 6.5–7.0 MJ/Nm^3 and CGE = 55–64% at ER = 0.20	[25]
Municipal solid waste, agricultural biomass	Waste Unused (agricultural residue)	Fixed-bed downdraft gasifier (5–100 kg/h, 3–60 kW)	T = 700–950 °C	Maximum electric load generated = 5 kW, with electrical efficiencies of 22, 20, and 19.5% at MSW ratios = 0, 20, and 40 wt.%, respectively	[26]
Wood waste (WW), chicken manure (CM)	Unused (wood) Waste	Fixed-bed downdraft gasifier (10 kg/h, 10 kW)	T = 800–900 °C	High-quality syngas is produced at CM/WW = 30 wt%/70 wt% with LHV = 5.23 MJ/Nm^3	[27]

CGE = cold gas efficiency; LHV = lower heating value; SD = sawdust, BD = bamboo dust; ER = equivalence ratio; WDC = wood chips; CS = coconut shells; WCF = wood-coconut fibres; CGR = co-gasification ratio; WW = wood waste; CM = chicken manure.

The woody terrestrial cultivated biomass for fuel includes willow, poplar, and eucalyptus, and gasification studies have been performed with samples of these species alone. Of these three, willow is particularly suitable for cultivation in Japan. In Japan, the extent

of abandoned farmland is increasing yearly. In 2015, abandoned farmland amounted to 42.3×10^4 hectares [29], and Fukushima Prefecture alone hosted 25.2×10^3 hectares [29]. Thus, developing measures for the utilisation of farmland is a significant issue. Willow is considered a promising biomass resource for addressing the challenges of securing stable domestic biomass fuels and utilising abandoned farmland. In particular, *Salix pet-susu Kimura* (ezonokinu willow, EW) (Figure 1a) is known for its high production rate among the fast-growing willow species. Its easy propagation, substantial initial growth, and sprouting regeneration potential offer advantages such as storage stability, production consistency, and business reliability. Consequently, they can be systematically and reliably produced over several years, with easy production adjustments.

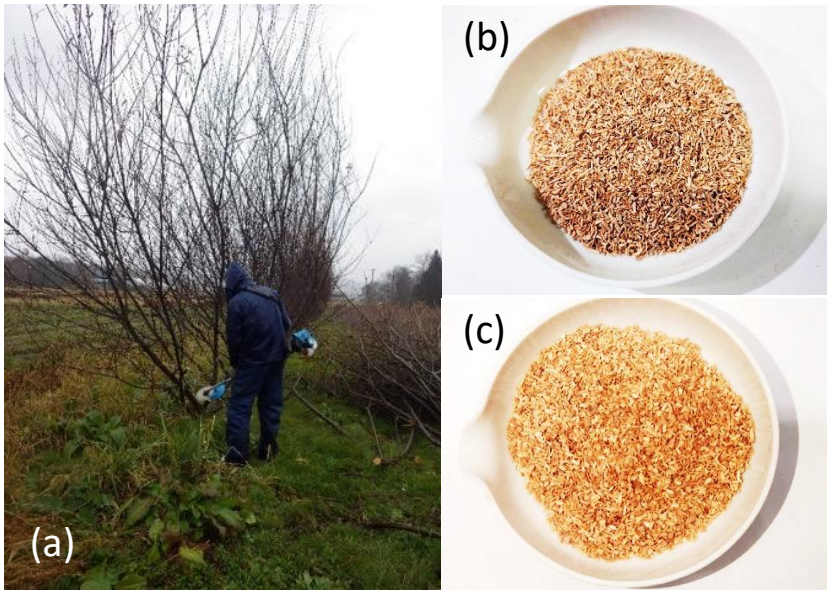

Figure 1. (**a**) Ezonokinu willow and its cuttings (5–6 cm diameter, ca. 1.1 dry-t/10 a) [30]; (**b**) crushed ezonokinu willow (with bark); (**c**) crushed cedar (without bark).

Morimoto et al. [30] conducted experiments in which they harvested EW with a mower (commonly used by farmers and foresters for weeding) and chipped it with a small crusher. Furthermore, when compared to Japanese cedar (*Cryptomeria japonica D.*), a typical Japanese plantation forest tree, EW has slightly higher ash content. However, its volatile matter content and ultimate analysis values are similar to those of Japanese cedar, making it a promising fuel for gasification. Nonetheless, the gasification reaction rate of willow is slower than that of cedar, which presents a challenge.

Therefore, this study aims to conduct a kinetic fuel characterisation of willow-cedar char mixtures to determine the extent of the synergistic effects of the mixture and the reaction pathways to increase the flexibility of feedstock (co-gasification) for the commercialisation of biomass-based gasification CHP systems.

2. Materials and Methods

2.1. Materials and Sample Preparation

The raw materials used in this study were ezonokinu willow (EW, Salix pet-susu Kimura clone KKD [31]) with its bark, grown in Kawasaki, Miyagi Prefecture (38°10′ N, 140°38′ E) (Figure 1b), and cedar without bark, obtained from the Shirakawa area in Fukushima Prefecture (Figure 1c). The results of the proximate, ultimate, and component analyses of EW and Japanese cedar are presented in Table 3. EW exhibits a slightly higher ash content than that of Japanese cedar, a representative plantation forest species in Japan. However, its volatile matter and ultimate analysis results are similar to those of Japanese cedar. This indicates its potential as a promising fuel for gasification.

Table 3. Results of proximate, ultimate, and compositional analyses of willow and cedar.

Sample	Proximate Analysis [wt%-db]			Ultimate Analysis [wt%-daf]						LHV [MJ/kg]	Component Analysis [wt%-daf]		
	VM	FC	Ash	C	H	N	S	Cl	O		Cellulose	Hemicellulose	Lignin
Cedar	80.2	19.4	0.4	52.5	5.85	0.07	<0.05	<0.02	41.4	19.6	47.9	19.9	31.7
Willow	80.4	17.7	1.90	49.6	5.93	0.81	<0.05	<0.02	41.7	18.4	34.0	37.0	27.9
Tomato SLs	71.6	14.2	14.2	41.3	5.23	2.96	0.96	0.12	36.0	15.1	12	12	15.1

LHV: lower heating value. SLs: stems and leaves.

To compare the gasification characteristics of biomass with different metal contents, tomato stems, and leaves were used as the reference biomass.

Willow was ground using a small hammer mill (RT-34, Ito Seisakusho Co., Ltd., Tokyo, Japan) and sieved to a particle size of 2.0–2.8 mm using a sieve shaker (Retsch AS200, Verder Scientific Co., Tokyo, Japan). Subsequently, the samples were dried at 105 °C for 24 h and under reduced pressure (−0.06 MPaG) for 24 h in a desiccator. Next, they were weighed using an electronic balance, with a target weight of 15.00 g, and pyrolysed in an argon (Ar) atmosphere with a flow rate of 400 mL/min. The temperature was increased to 800 °C at a rate of 10 K/min. The obtained willow char (WC) was ground in an agate mortar, sieved to a particle size of 0.075–0.25 mm and then dried under reduced pressure (−0.06 MPaG) in a desiccator. This exact procedure was also applied to cedar and tomato stems and leaves. The char samples obtained from cedar, willow, and tomato stems and leaves were, respectively, labelled as cedar char (CC), WC, and tomato stems and leaves char (TC), respectively.

2.2. Experimental and Analytical Methods

Char samples prepared using the preparation method described in the previous section were utilised in the CO_2 gasification test with TG-DTA as the analyser (Thermo Plus EVO2-FKH, RIGAKU, Kyoto, Japan). After placing 6 mg of the sample on a platinum pan and inserting it into a sample holder, the reaction temperature was raised to 800 °C at a heating rate of 30 °C/min, with Ar supplied as the atmosphere gas at a flow rate of 400 mL/min. Subsequently, the gas was switched to CO_2 gas, supplied at a flow rate of 400 mL/min, and maintained at 800 °C until the reaction was completed. Reaction kinetic analysis was conducted by analysing the obtained TG and DTA curves. A binary mixture sample of char was prepared by placing the char sample in a platinum pan and stirring it 20 times, alternating between left- and right-handed rotations using a wire. Hence, the blend ratio of the two types of biochar was determined using the following blend ratio.

$$\text{WC blend ratio [wt\%]} = \frac{\text{Willow char [g]}}{\text{Willow char [g]} + \text{Cedar char[g]}} \times 100 \quad (1)$$

The bulk density of the char samples was determined by placing samples with a particle size of 75–250 μm in a platinum pan (Φ 5 × 5 mm, 100 μL) used for TG-DTA and measuring their mass.

A chemisorption-physisorption analyser (AUTOSORB-1-C, Quantachrome Instruments, Boynton Beach, FL, USA) was employed to determine BET-specific surface area, pore volume, and average pore size in gas adsorption experiments. For the measurement, 0.1 g of pre-dried char sample was used. After 3–5 h of pre-treatment, measurements were conducted in a nitrogen gas atmosphere at a temperature of 77 K ranging from 0.01–1.0 relative pressure, while adsorption isotherms were generated. BET plots analysed using data from gas adsorption experiments on five types of char ranging from 0.05–0.3 relative pressure were used to determine BET-specific surface area S [m^2/g], pore volume V [cm^3/g], and average pore diameter D [nm]. These were calculated from the amount of nitrogen adsorbed at a relative pressure of 0.98. Table 4 presents the results of the gas adsorption analysis of the char samples (CC, WC, and TC).

Table 4. Results of gas adsorption analysis.

Char Sample	Atmospheric Gas	BET-Specific Surface Area, S (m^2/g)	Pore Volume, V (cm^3/g)	Mean Pore Diameter, D (nm)	r_p/λ (DI)	Gas Diffusion
Cedar (This study)	Ar	309	0.1439	18.61	0.050	Knudsen
Willow (This study)	Ar	277	0.1326	19.18	0.052	Knudsen
Douglas fir char [32]	N_2	275	0.15	2.2	0.006	Knudsen
Douglas fir char [32]	N_2:18%/CO_2:41%/ O_2:41%	417	0.24	2.3	0.006	Knudsen
Peachtree branch [33]	N_2	112	0.0311	2.60	0.007	Knudsen
Persimmon tree branch [33]	N_2	36.5	0.032	4.16	0.011	Knudsen
Cherry tree branch [33]	N_2	234	0.0298	2.32	0.006	Knudsen
Zelkova tree branch [33]	N_2	137	0.0474	3.10	0.008	Knudsen
Timber waste [33]	N_2	8.11	0.0126	6.22	0.017	Knudsen

The surface of the char samples was observed using a scanning electron microscope (SEM; SU8000, HITACHI, Tokyo, Japan). The results of the SEM observations of the pore structure of CC, WC, and TC are shown in Figure 2.

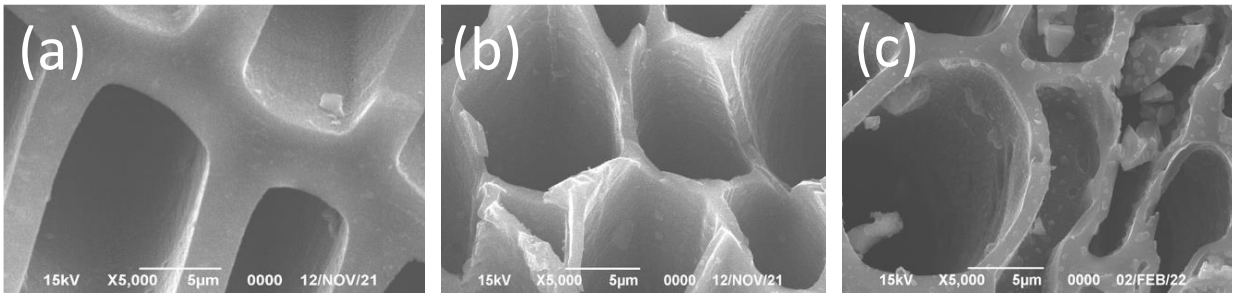

Figure 2. Pore structure of char samples: (**a**) CC; (**b**) WC; (**c**) TC.

The composition of ash in the char was determined using an X-ray fluorescence analyser (XRF, Rigaku, RIX1000, Tokyo, Japan); the oxide-based inorganic composition (wt%) obtained from the XRF measurements is presented in Table 5.

Table 5. Results of ash chemical composition analysis by XRF.

Char Sample	Chemical Composition [%] (Oxide Basis)											
	SiO_2	P_2O_5	Fe_2O_3	Al_2O_3	CaO	MgO	Na_2O	K_2O	Cl	SO_3	ZnO	CuO
CC	3.10	3.14	0.943	1.70	23.6	4.81	4.37	57.8	0.02	1.67	0.0124	0.0125
WC	3.08	23.7	0.886	1.36	38.2	4.39	0.863	25.8	0.02	3.15	0.324	0.025
TC	2.57	11.8	0.972	1.34	16.9	5.06	2.70	70.8	0.77	8.64	0.0124	0.0125

CC = cedar ash; WC = willow ash; TC = tomato stem and leaf ash.

3. Kinetic Theory

The RPM [34], a gas-solid reaction model, was employed to analyse reaction kinetics in char gasification. RPM assumes the random presence of cylindrical pores within the solid, and it is expressed as follows:

$$\frac{dX}{dt} = k_p(1-X)\sqrt{1-\Psi \cdot ln(1-X)} \quad (2)$$

where X is the conversion rate defined by

$$X = X_{exp} = \frac{m_0 - m}{m_0 - m_f} \quad (3)$$

where m denotes the weight of the char sample, m_0 represents the initial weight of the char sample, and m_f denotes the final weight of the char sample. Solving Equation (2) analytically for X yields Equation (4):

$$X = 1 - exp\left|-k_p t\left(1 + \frac{\Psi k_p}{4} t\right)\right| \quad (4)$$

Taking the logarithm to the terms on both sides of Equation (4) yields the following equation:

$$\frac{-ln(1-X)}{t} = K_p + \frac{\Psi k_p^2}{4} t \quad (5)$$

In the char gasification test conducted under isothermal conditions by TG, a graph of $-\ln(1 - X)/t$ and t was plotted using Microsoft® Excel for Mac version 16.87. The gasification reaction rate k_p and the pore structure parameter Ψ were determined using the intercept and slope of the graph.

4. Results and Discussion

4.1. Fuel Characterisation of Different Chars

4.1.1. Effect of Pore Structure and CO_2 Diffusion on Gasification Rate

The TG and reaction rate results for WC alone, CC alone, and TC alone are shown in Figures 3a and 3b, respectively. Figure 3a,b show that TC exhibited a rapid weight loss compared to the other samples, with a reaction time of 14 min, while the reaction times for CC and WC were 72 min and 241 min, respectively. Regarding the reaction rate, TC, similar to WC and CC, displayed an upward convex distribution with a peak at X = 0.73 in the second half of the reaction. The ash content of tomato stems and leaves was 14.2%, which was higher than that of other samples (cedar: 0.4%, EW: 1.90%). Furthermore, the composition of reaction-promoting AAEMs, such as K and Ca, was 70.8% and 16.9%, respectively, which was also higher than in the other samples.

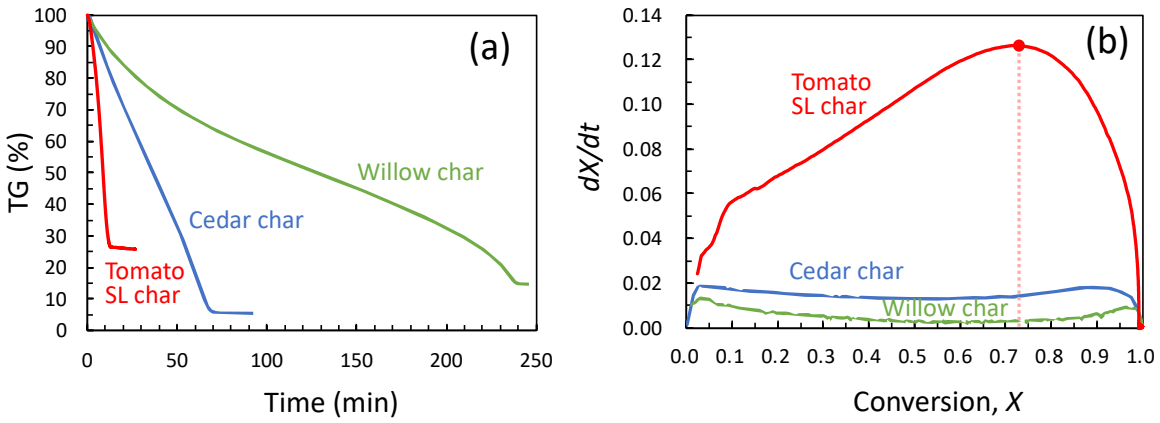

Figure 3. Comparison of (**a**) TG results and (**b**) reaction rates (dX/dt) for different biomass species (CC, WC, and TC). Points on the reaction rate curve of TC indicate the apex.

The pore structures of CC, WC, and TC were observed using an SEM, and the results are depicted in Figure 2. A comparison of the characteristics of the char samples obtained from the analysis of these images is presented in Table 6.

Table 6. Summary of observations of biomass char cell walls using SEM and bulk density.

Sample	Pore Section	Cell Wall Thickness (μm)	Bulk Density (kg/m^3)
CC	Rectangles	~3.0	140
WC	Hexagons	~1.5	400
TC	Complex shapes	~1.3	160

Figure 2 and Table 6 show that the pore shapes were rectangular in CCs, hexagonal in WCs, and complex in TCs. The cell wall thickness measured approximately 3.0 μm for CC, 1.5 μm for WC, and 1.3 μm for TC, with CC having the thickest structure. Conversely, the bulk densities were 140 kg/m^3 for CC, 400 kg/m^3 for WC, and 160 kg/m^3 for TC, with CC having the lowest value.

In conjunction with the results obtained from SEM observations, gas adsorption experiments were conducted to provide a more detailed comparison of the pore structures. The results are presented in Table 4, which show that the specific surface area and pore volume of CC and WC are larger, while the average pore diameter of WC is slightly larger. The diffusion indicator (DI) value represents the predicted gas diffusion pattern within the pores [32] and is defined by the following equations:

$$\text{Mean free path}: \ \lambda = \frac{1}{\sqrt{2}\pi\left(\frac{N_A}{V}\right)d^2} \tag{6}$$

$$\text{Diffusion Indicator}: \ \text{DI} = \frac{r_p}{\lambda} \tag{7}$$

where V is the pore volume, d is the CO_2 molecular diameter (0.44 nm), r_p is the average pore radius, and N_A is the Avogadro constant (6.02×10^{23} mol^{-1}). The diffusion of CO_2 in WC and CC char pores exhibits Knudsen diffusion for DI < 0.1, transitional diffusion for $0.1 \leq \text{DI} \leq 10$, and molecular diffusion for DI > 10. If CO_2 diffusion into the pores is Knudsen diffusion, it is unsuitable for CO_2 gasification. WC and CC have a small pore diameter of 19 mm, DI = 0.05 (<0.1), indicating Knudsen diffusion, and gas molecules in the pores are dilute.

The mean pore diameter conditions for Knudsen diffusion in the gasification of char with CO_2 are considered here. Substituting Equation (7), $D = 2\ r_{p,}$ and λ = 170–202 nm (T = 800–1000 °C) for the Knudsen diffusion condition DI < 0.1, we obtain D < 34–40 nm. This result suggests that pores with diameters smaller than 40 nm may be less reactive during CO_2 gasification.

4.1.2. Effect of Reaction Temperature on Gasification Rate

The results of the time variation of the conversion rate X for WC at reaction temperatures of 800, 900, and 1000 °C are shown in Figure 4a. At reaction temperatures of 800, 900, and 1000 °C, the reaction times were 239 min, 25 min, and 10 min, respectively. The results for the reaction rate (dX/dt) of WC at reaction temperatures of 800, 900, and 1000 °C are shown in Figure 4b. It was found that the increase in the reaction rate dX/dt after the conversion ratio X = 0.8 markedly increased with increasing reaction temperature. In the early to middle stages of the reaction (X = 0.1 to 0.7), the reaction rate at 1000 °C increased to about 13 times higher than that at 800 °C and about 2.5 times higher than that at 900 °C. At the end of the reaction phase (X = 0.7 to 1.0), the reactivity at 1000 °C increased to about 30 times higher than that at 800 °C and about six times higher than that at 900 °C.

The results illustrating the dependence of the reaction rate constant k_p and the pore structure parameter Ψ on the reaction temperature for the gasification of WC with CO_2 are shown in Figure 4c. The reaction rate constant k_p exhibited an upward trend with increasing reaction temperature, while the pore structure parameter Ψ exhibited a sharp increase from 900 to 1000 °C.

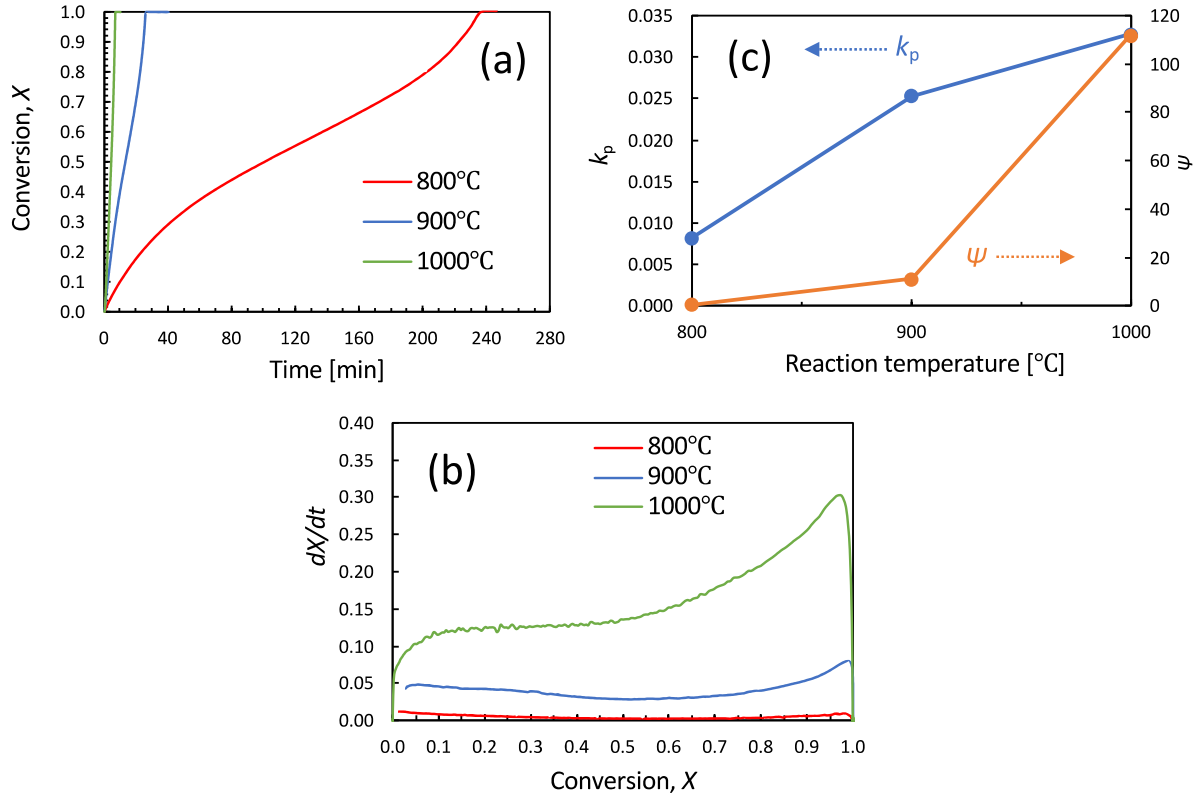

Figure 4. Effect of reaction temperature on (**a**) carbon conversion X, (**b**) reaction rate dX/dt, and (**c**) reaction rate constant k_p and pore structure parameter Ψ in the gasification of WC.

4.2. Fuel Characterisation of the Blended Char

4.2.1. Kinetics of the Blended Char Co-Gasification in CO_2

The results for the conversion ratio X for the WC and CC blends are depicted in Figure 5a, where $X = 0$ indicates the start of the reaction and $X = 1$ indicates the end of the reaction. The higher the WC blend ratio, the slower the progress of the reaction. The reaction rate (dX/dt) results are presented in Figure 5b. For WC alone (blend ratio = 100%), a rapid increase in the reaction rate was observed after a conversion ratio of $X = 0.8$. The samples with a WC blend ratio of 60–100 wt% exhibited a similar distribution of reaction rates after the conversion ratio $X = 0.7$. This is because, as seen in Figure 5a, WC remains until the late reaction phase due to its slow reaction, causing the gasification reaction of this remaining WC to dominate after the conversion ratio X = 0.7.

The calculated reaction rate constant k_p and pore structure parameter Ψ are displayed in Figure 5c. With increasing WC blend ratio, the reaction rate constant k_p increased slowly and showed a peak at 50 wt%. The pore structure parameter Ψ decreased as the WC blend ratio increased and remained relatively constant after reaching 50 wt%. The highest pore structure parameter (11.76) was observed for CC alone at BR = 0 wt%. As char gasification is a surface reaction, the pore structure, specific surface area, surface functional groups, and inorganic components of the char may influence the reaction rate. Therefore, TC was used as a reference sample to analyse the pore structure.

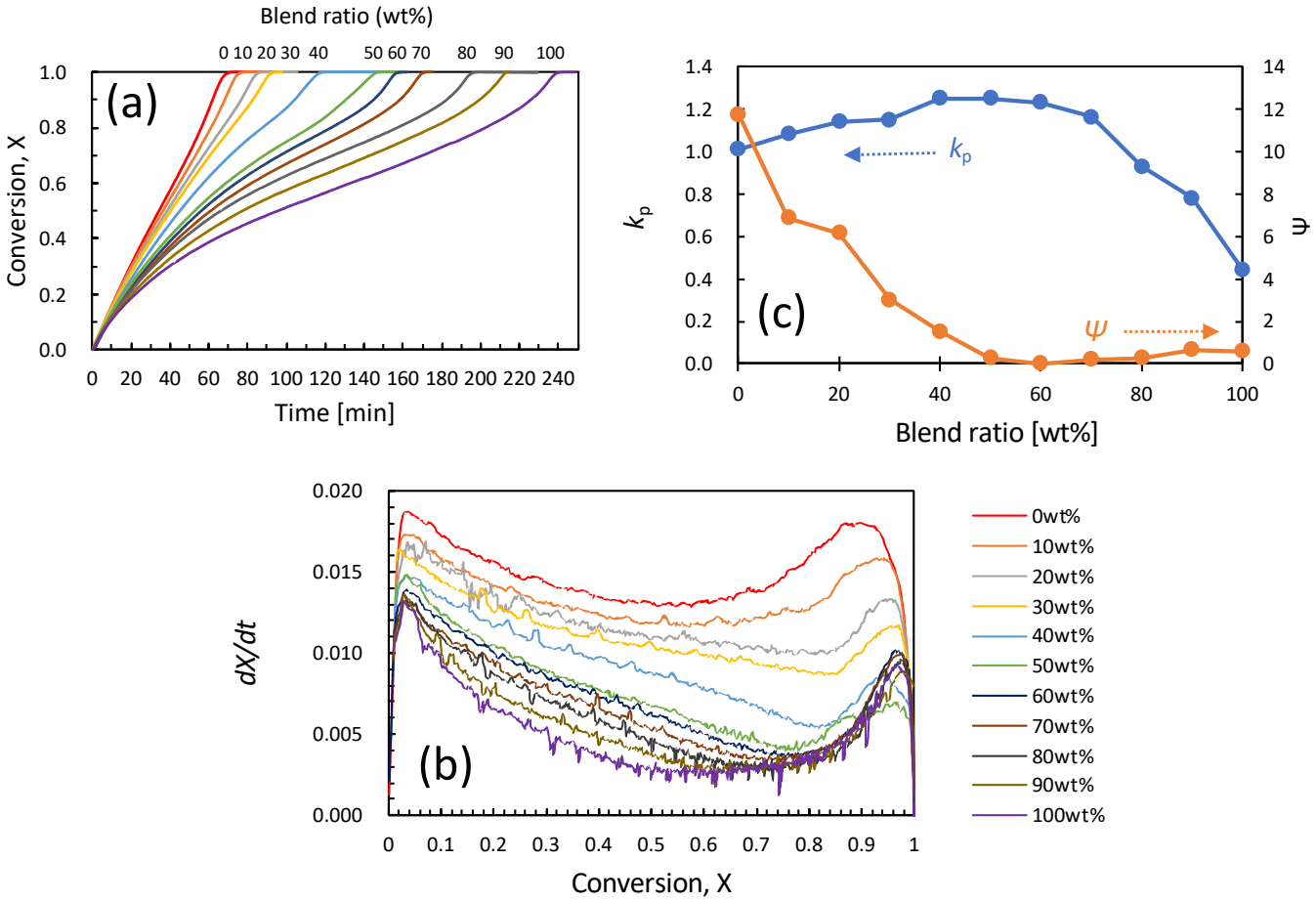

Figure 5. Comparison of (**a**) conversion X, (**b**) reaction rate (dX/dt), and (**c**) reaction rate constant k_p and pore structure parameter Ψ for CO_2 gasification at various Ezonokinu WC blends.

4.2.2. Effect of Char Structure and AAEM on Reactivity

The relationship between the reactivity (reaction rate at $X = 0.1$, $dX/dt\mid_{X=0.1}$) and specific surface area is shown in Figure 6a. The ($dX/dt\mid_{X=0.1}$) values obtained using TG-DTA for the various blend ratios of chars were plotted against the specific surface area, showing a strong positive correlation with a correlation coefficient of $r = 0.806$. Therefore, it is suggested that the specific surface area influences the rate of CO_2 gasification reaction in the early stages of the reaction.

The relationship between the pore structure parameter Ψ and $dX/dt\mid_{X=0.1}$ is depicted in Figure 6b. The values of the pore structure parameter Ψ were obtained by fitting RPM to the reactivity of WC and CC for CO_2 gasification. The correlation coefficient between $dX/dt\mid_{X=0.1}$ and Ψ was $r = 0.851$ with a quadratic curve from Figure 6b, indicating a strong positive correlation. Therefore, it is suggested that the pore structure strongly influences the first half of the reaction.

The relationship between the bulk density and $dX/dt\mid_{X=0.1}$ is shown in Figure 6c. Here, the bulk densities of WC, CC, and TC were used to calculate the correlation coefficient with the initial reactivity in the gasification reaction, which was $r = -0.519$, confirming a negative correlation.

The chemical compositions of the inorganic elements obtained through XRF analysis are presented in Table 5. Si and Al are considered inhibitors in CO_2 gasification, while K has a reaction-promoting effect, and Ca has an equivalent or slightly promoting effect at high temperatures of 1000 °C and 1500 °C [35]. The SiO_2 and Al_2O_3 contents are relatively low, and their influence on gasification in the present study is considered to be minor. Therefore, the focus was placed on K_2O and CaO, which have relatively high content.

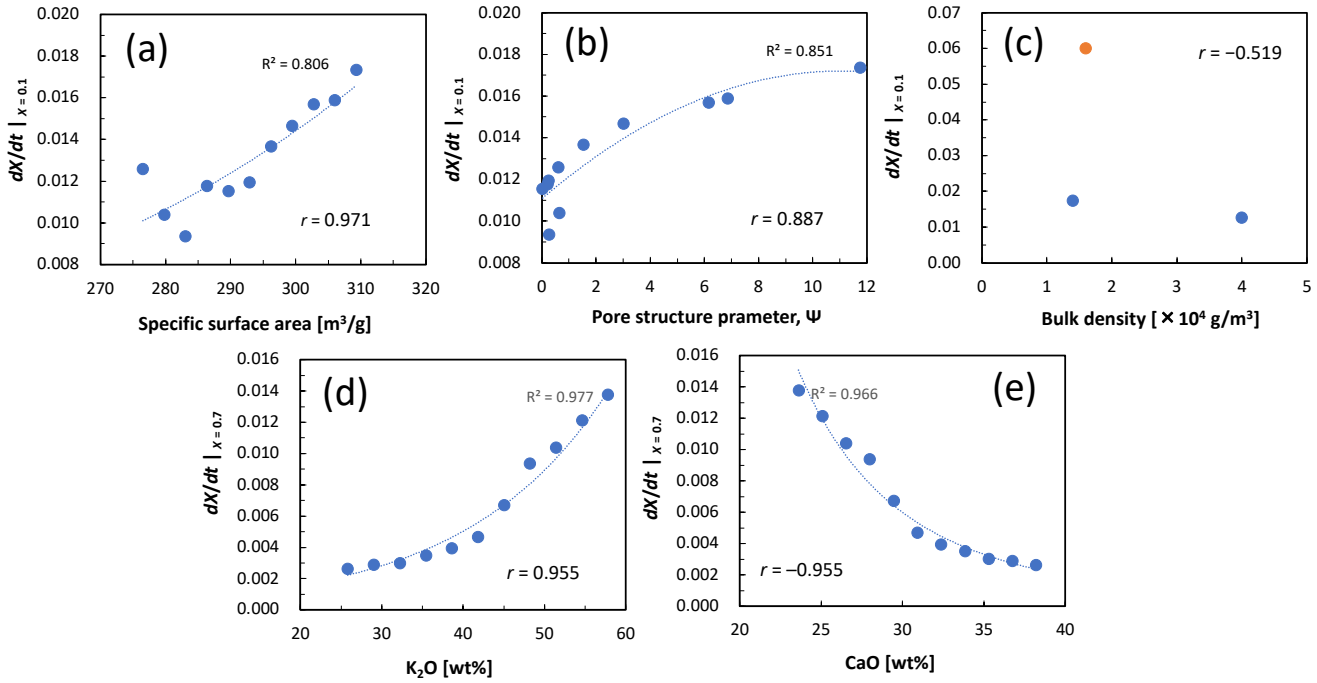

Figure 6. Relationship between (**a**) specific surface area and reactivity $dX/dt\,|_{X=0.1}$; (**b**) pore structure parameter Ψ and reactivity $dX/dt\,|_{X=0.1}$; (**c**) bulk density and reactivity $dX/dt\,|_{X=0.1}$; (**d**) K_2O content and reactivity $dX/dt\,|_{X=0.7}$; and (**e**) CaO content and reactivity $dX/dt\,|_{X=0.7}$ (blue plot: WC/CC; orange-coloured plot: TC).

The relationship between the content of K_2O and CaO and $dX/dt\,|_{X=0.7}$ is shown in Figure 6d,e, utilising the values for CC and WC with blend ratio as presented in Table 5 for K_2O or CaO content. By observing the correlation between $dX/dt\,|_{X=0.7}$ and K_2O/CaO content, we can clarify the influence of K_2O and CaO on reactivity, and these correlations are plotted in Figure 6d,e.

Figure 6d shows that $dX/dt\,|_{X=0.7}$ tends to increase as K_2O increases, with a strong positive correlation indicated by the correlation coefficient $r = 0.955$. Therefore, K_2O is responsible for enhancing the reaction at the end of the reaction phase. On the contrary, as shown in Figure 6e, $dX/dt\,|_{X=0.7}$ decreases exponentially with an increase in CaO, demonstrating a strong negative correlation with a correlation coefficient of $r = -0.955$. Consequently, CaO inhibited the reaction at the end of the reaction phase.

In conclusion, the factors affecting the CO_2 gasification of char in the early stages of the reaction are the specific surface area and pore structure parameters. In contrast, the factors influencing the reaction in the later stages are inorganic components, such as K_2O and CaO.

4.3. Synergistic Effect of Char Blends

To quantitatively analyse the change in the synergy factor [14] as the co-gasification of the WC and CC blended sample progresses in Figure 7, the synergy factor [14] is defined as follows:

$$A_{x,T} = \frac{t_{x,T,cal}}{t_{x,T,exp}} \tag{8}$$

where $t_{x,T,\mathrm{exp}}$ is the reaction time required for the experimental conversion rate $X_{\mathrm{exp}} = 0$ to $X_{\mathrm{exp}} = x$ (Equation (3)). $t_{x,T,\mathrm{cal}}$ is the reaction time required for the calculated conversion rate $X_{\mathrm{cal}} = 0$ to $X_{\mathrm{cal}} = x$, assuming no sample interaction during CO_2 gasification. (The calculated conversion X_{cal} is determined from the weight curves obtained by weighted-averaging the weights of WC alone and CC alone with the blend ratio.)

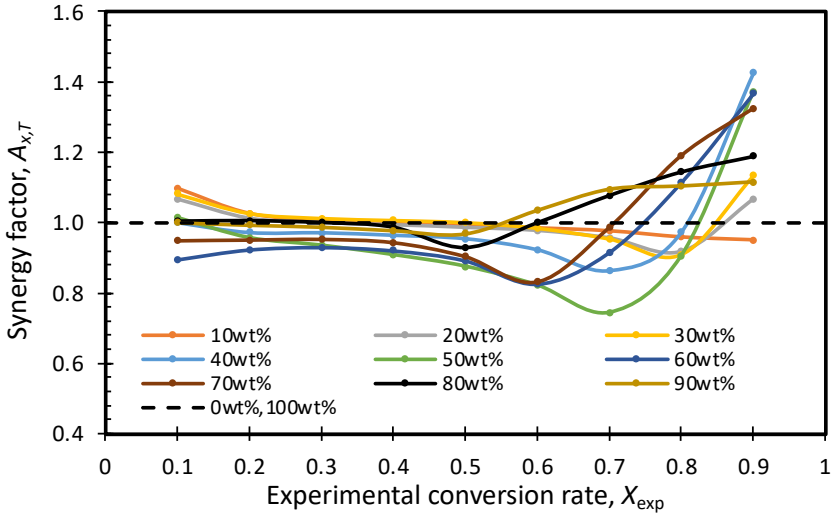

Figure 7. Changes in synergy factors with various blend ratios.

Figure 7 shows that the synergy factor remained relatively constant at 1 as the conversion rate increased in all cases with a WC blend ratio ranging from 20 to 90 wt%, and subsequently decreased temporarily before gradually increasing again, ultimately exceeding a value of 1. The most significant negative peak of the synergy factor was observed in the case of a 50 wt% WC blend ratio, where it dropped to 0.74 at a conversion rate of $X = 0.7$. Additionally, as the WC blend ratio increased, the negative peak of the synergy factor shifted toward lower conversion rates. This suggests that during CO_2 gasification of the CC/WC blended char samples, the carbon content of the faster-reacting CC was initially depleted, followed by that of WC and cedar ash. The primary components of cedar ash, calcium (Ca) and potassium (K), subsequently melted and coated the WC pores, thereby inhibiting the Boudouard reaction (R5), which is the surface reaction of CO_2 gas with the WC pores. Notably, the generation of a melt due to eutectic crystallisation was observed in melting tests of $CaCO_3$-K_2CO_3 mixed samples [36]. Subsequently, a pathway for CO_2 to penetrate the char gradually opens up, and conversely, the inorganic components in the cedar ash accelerate the reaction [35]. This phenomenon is believed to have led to a rapid increase in the synergy index. Figure 8 illustrates the reaction pathway for the co-gasification of willow/cedar blended chars.

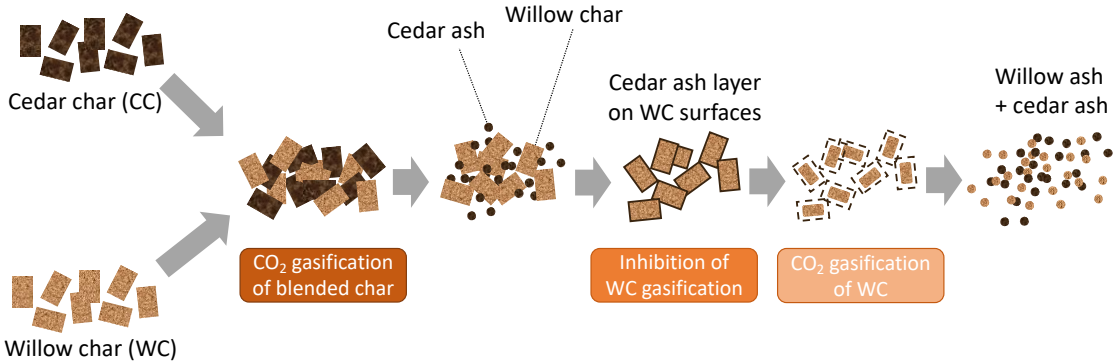

Figure 8. Proposed reaction pathway for CO_2 co-gasification of willow/cedar blended chars.

A synergistic effect, which seems to originate from the pores, was observed even in the early stages of the reaction. In char gasification, the reaction primarily occurs on the char surface. Therefore, from the early to mid-phase of the reaction ($X = 0.1$–0.7), the unique structure of the char (specific surface area and pore shape) is considered to influence CO_2 gasification. The carbon within the char is gasified to some extent by atmospheric

CO_2, which later exposes the ash content. Consequently, it is suggested that the inorganic components in the ash influence gasification in the latter stages of the reaction (0.7–0.9).

In previous studies, blended coal and woody biomass chars were produced by pyrolysis of a mixture of pulverised coal and pulverised woody biomass, co-gasification of the blended chars was performed, and fuel characterisation was conducted. [11–14]. Gasification of rice straw-bituminous coal blend chars showed that the inhibition effect first weakened, and then the synergistic effect increased with increasing conversion. In the case of rice straw-anthracite blends, the synergistic effect was strong in the early stages, peaked in the mid-term, and then weakened. Synergies in rice straw-bituminous coal blends were due to active K and Ca transformations and correlated with active K transformations in rice straw-anthracite blends [14]. Juntao Wei et al. [13] investigated the reactivity of co-gasification of petroleum coke and biomass using TGA. The results showed that the synergistic effect of co-gasification weakened at 1100 °C. This phenomenon correlates with the appearance of potassium-rich molten biomass ash in the glassy state.

In summary, the results of the synergy factors for willow/cedar blended char co-gasification suggest that during the first half of the reaction, the pore size and specific surface area affect the reaction rate. In contrast, in the later stages of the reaction, the effects of inorganic components on both promoting and inhibiting co-gasification become influential. The reaction pathway is indicated by the synergy factors observed in the co-gasification of willow/cedar blended char.

The results obtained using TG-DTA were based on the small size and small amounts of pyrolysed char samples. Therefore, the analysis results show the influence of the char pore structure and AAEM on the microscopic reaction rate. However, the influence of feedstock size on the reaction needs to be investigated using larger feedstock samples, as feedstock particles are larger with gasification in practice.

In industrial applications of fixed-bed gasification CHP systems with EW/Cedar, a larger system is not necessarily appropriate, as EW biomass is a local agricultural residue and should be used on a small and decentralised scale. For sustainable energy production, installing many CHP systems as decentralised heat sources for local communities is important. However, one of the challenges of small-scale installations is their low profitability. The added value of the agricultural use of pyrolysis residues effectively solves this low profitability and optimises the entire system, including not only woody biomass energy production but also the related peripheral processes. The conversion efficiency of woody biomass energy is higher than that of large-scale steam turbine power generation, which means that the GHG reduction per unit of woody biomass is also higher, making the system more effective in reducing greenhouse gases.

5. Conclusions

For the commercial operation of cedar/willow-fuelled gasification combined with heat and power plants in Japan, kinetic investigation of CO_2 gasification of the blended chars is essential. However, unutilised and cultivated biomass remains uninvestigated. Kinetic analysis by TG-DTA, chemical composition analysis of ash by XRF, surface observation by SEM, and analysis of CO_2 diffusion in the pores by a gas adsorption analyser revealed the following gasification behaviour of cedar and willow char.

- The pore size and specific surface area influence the reaction rate of CO_2 gasification in the early and middle stages of co-gasification of willow and cedar blended char. This is followed by K-induced reaction enhancement and Ca-induced reaction inhibition in the final stages of the reaction.
- In the CO_2 co-gasification of willow and cedar blended char, the reaction is slow in the initial stages owing to Knudsen's diffusion of CO_2 into the char pore.
- CC, with a relatively fast reaction rate, first gasifies, and the remaining cedar ash forms a melt that inhibits the CO_2 gasification of the WC. However, CO_2 enters the pores of the WC, and gasification proceeds until it is completed.

- Our findings provide a deeper understanding of biomass co-gasification dynamics, which is pivotal for optimising gasification processes and improving the efficiency of biomass utilisation.

Author Contributions: Conceptualisation, K.K.; methodology, K.K. and K.E.; software, K.K. and K.E.; validation, K.K. and K.E.; formal analysis, K.K. and K.E.; investigation, K.E.; resources, K.K., H.M., and H.O.; data curation, K.K. and K.E.; writing—original draft preparation, K.E.; writing—review and editing, K.K. and H.O.; visualisation, K.K. and K.E.; supervision, K.K. and M.S.; project administration, K.K.; funding acquisition, K.K. All authors have read and agreed to the published version of the manuscript.

Funding: This work was supported by JSPS KAKENHI Grant Number 23K11500.

Data Availability Statement: The original contributions presented in the study are included in the article, and further enquiries can be directed to the corresponding author.

Conflicts of Interest: The authors declare no conflicts of interest.

References

1. Koido, K.; Iwasaki, T.; Kurosawa, K.; Takaku, R.; Ohashi, H.; Sato, M. Cesium-Catalyzed Hydrogen Production by the Gasification of Woody Biomass for Forest Decontamination. *ACS Omega* **2021**, *6*, 5233–5243. [CrossRef] [PubMed]
2. Koido, K.; Ogura, T.; Matsumoto, R.; Endo, K.; Sato, M. Spent Mushroom Substrate Performance for Pyrolysis, Steam Co-Gasification, and Ash Melting. *Biomass Bioenergy* **2021**, *145*, 105954. [CrossRef]
3. Koido, K.; Kurosawa, K.; Endo, K.; Sato, M. Catalytic and Inhibitory Roles of K and Ca in the Pyrolysis and CO_2 or Steam Gasification of Erianthus, and Their Effects on Co-Gasification Performance. *Biomass Bioenergy* **2021**, *154*, 106257. [CrossRef]
4. Roncancio, R.; Gore, J.P. CO_2 Char Gasification: A Systematic Review from 2014 to 2020. *Energy Convers. Manag. X* **2021**, *10*, 100060. [CrossRef]
5. Phounglamcheik, A.; Wang, L.; Romar, H.; Kienzl, N.; Broström, M.; Ramser, K.; Skreiberg, Ø.; Umeki, K. Effects of Pyrolysis Conditions and Feedstocks on the Properties and Gasification Reactivity of Charcoal from Woodchips. *Energy Fuels* **2020**, *34*, 8353–8365. [CrossRef]
6. Asadullah, M.; Zhang, S.; Min, Z.; Yimsiri, P.; Li, C.Z. Effects of Biomass Char Structure on Its Gasification Reactivity. *Bioresour. Technol.* **2010**, *101*, 7935–7943. [CrossRef] [PubMed]
7. Mei, Y.; Wang, Z.; Zhang, S.; Fang, Y. Novel Assumption about the Mechanism of Catalytic Gasification: On the Basis of the Same Catalytic Effect of Alkali between C–CO_2 and Fe–CO_2 Reactions. *Energy Fuels* **2021**, *35*, 16258–16263. [CrossRef]
8. Yu, J.; Guo, Q.; Gong, Y.; Ding, L.; Wang, J.; Yu, G. A Review of the Effects of Alkali and Alkaline Earth Metal Species on Biomass Gasification. *Fuel Process. Technol.* **2021**, *214*, 106723. [CrossRef]
9. Dahou, T.; Defoort, F.; Jeguirim, M.; Dupont, C. Towards Understanding the Role of K during Biomass Steam Gasification. *Fuel* **2020**, *282*, 118806. [CrossRef]
10. Li, X.; He, J.; Liu, M.; Bai, J.; Bai, Z.; Li, W. Interaction between Coal and Biomass during Co-Gasification: A Perspective Based on the Separation of Blended Char. *Processes* **2022**, *10*, 286. [CrossRef]
11. Jeong, H.J.; Park, S.S.; Hwang, J. Co-Gasification of Coal-Biomass Blended Char with CO_2 at Temperatures of 900–1100 C. *Fuel* **2014**, *116*, 465–470. [CrossRef]
12. Jeong, H.J.; Hwang, I.S.; Hwang, J. Co-Gasification of Bituminous Coal-Pine Sawdust Blended Char with H_2O at Temperatures of 750–850 °C. *Fuel* **2015**, *156*, 26–29. [CrossRef]
13. Wei, J.; Guo, Q.; Gong, Y.; Ding, L.; Yu, G. Synergistic Effect on Co-Gasification Reactivity of Biomass-Petroleum Coke Blended Char. *Bioresour. Technol.* **2017**, *234*, 33–39. [CrossRef]
14. Wei, J.; Gong, Y.; Guo, Q.; Chen, X.; Ding, L.; Yu, G. A Mechanism Investigation of Synergy Behaviour Variations during Blended Char Co-Gasification of Biomass and Different Rank Coals. *Renew. Energy* **2019**, *131*, 597–605. [CrossRef]
15. Zuo, H.B.; Geng, W.W.; Zhang, J.L.; Wang, G.W. Comparison of Kinetic Models for Isothermal CO_2 Gasification of Coal Char-Biomass Char Blended Char. *Int. J. Miner. Metall. Mater.* **2015**, *22*, 363–370. [CrossRef]
16. Gomez, R.D.; Palacio, M.; Arango, J.F.; Avila, A.E.; Mendoza, J.M. Evaluation of the Energy Generation Potential by an Experimental Characterization of Residual Biomass Blends from Córdoba, Colombia in a Downdraft Gasifier. *Waste Manag.* **2021**, *120*, 522–529. [CrossRef]
17. Mallick, D.; Mahanta, P.; Moholkar, V.S. Co-Gasification of Biomass Blends: Performance Evaluation in Circulating Fluidized Bed Gasifier. *Energy* **2020**, *192*, 116682. [CrossRef]
18. Inayat, M.; Sulaiman, S.A.; Kurnia, J.C. Catalytic Co-Gasification of Coconut Shells and Oil Palm Fronds Blends in the Presence of Cement, Dolomite, and Limestone: Parametric Optimization via Box Behnken Design. *J. Energy Inst.* **2019**, *92*, 871–882. [CrossRef]
19. Sulaiman, S.A.; Roslan, R.; Inayat, M.; Yasin Naz, M. Effect of Blending Ratio and Catalyst Loading on Co-Gasification of Wood Chips and Coconut Waste. *J. Energy Inst.* **2018**, *91*, 779–785. [CrossRef]

20. Umar, H.A.; Sulaiman, S.A.; Said, M.A.; Gungor, A.; Ahmad, R.K.; Inayat, M. Syngas Production from Gasification and Co-Gasification of Oil Palm Trunk and Frond Using a down-Draft Gasifier. *Int. J. Energy Res.* **2021**, *45*, 8103–8115. [CrossRef]
21. Tamili, N.; Chuan, L.K.; Sulaiman, S.A.; Moni, M.N.Z.; Inayat, M.; Lo, M.Y.K. Co-Gasification of Corn and Coconut Residues in Downdraft Gasifier. *MATEC Web Conf.* **2018**, *225*, 04001. [CrossRef]
22. Monir, M.U.; Khatun, F.; Abd Aziz, A.; Vo, D.V.N. Thermal Treatment of Tar Generated during Co-Gasification of Coconut Shell and Charcoal. *J. Clean. Prod.* **2020**, *256*, 120305. [CrossRef]
23. Król, D.; Poskrobko, S. Experimental Study on Co-Gasification of Wood Biomass and Post-Extraction Rapeseed Meal: Methane-Rich Gasification. *Energy Fuels* **2017**, *31*, 3935–3942. [CrossRef]
24. Wiyono, A.; Ika Pratiwi, T.P.S.; Rianti Priadi, C.; Surjosatyo, A.; Dafiqurrohman, H. Investigation of Co-Gasification Characteristics of Wood-Coconut Fibers Pellet and Rice Husk Mixtures in a Downdraft Fixed Bed Gasifier. *Int. J. Technol.* **2017**, *8*, 1207. [CrossRef]
25. Bhoi, P.R.; Huhnke, R.L.; Kumar, A.; Indrawan, N.; Thapa, S. Co-Gasification of Municipal Solid Waste and Biomass in a Commercial Scale Downdraft Gasifier. *Energy* **2018**, *163*, 513–518. [CrossRef]
26. Indrawan, N.; Thapa, S.; Bhoi, P.R.; Huhnke, R.L.; Kumar, A. Electricity Power Generation from Co-Gasification of Municipal Solid Wastes and Biomass: Generation and Emission Performance. *Energy* **2018**, *162*, 764–775. [CrossRef]
27. Ng, W.C.; You, S.; Ling, R.; Gin, K.Y.H.; Dai, Y.; Wang, C.H. Co-Gasification of Woody Biomass and Chicken Manure: Syngas Production, Biochar Reutilization, and Cost-Benefit Analysis. *Energy* **2017**, *139*, 732–742. [CrossRef]
28. Zhu, Y.; Piotrowska, P.; Van Eyk, P.J.; Boström, D.; Wu, X.; Boman, C.; Broström, M.; Zhang, J.; Kwong, C.W.; Wang, D.; et al. Fluidized Bed Co-Gasification of Algae and Wood Pellets: Gas Yields and Bed Agglomeration Analysis. *Energy Fuels* **2016**, *30*, 1800–1809. [CrossRef]
29. Ministry of Agriculture Forestry and Fisheries of Japan Census of Agriculture and Forestry. Available online: https://www.e-stat.go.jp/en/stat-search?page=1&toukei=00500209&survey=Census%20of%20Agriculture%20and%20Forestry (accessed on 22 May 2024).
30. Morimoto, H.; Satoh, S.; Koido, K. A Simplified Method of Harvesting Willow Crops Cultivated as an Energy Source in Short Rotation Coppices in Small-Scale Farmlands. *J. Jpn. Inst. Energy* **2016**, *95*, 152–155. [CrossRef]
31. Satoh, S.; Ishizawa, K.; Mitsui, Y.; Minato, K. Growth and Above-Ground Biomass Production of a Willow Clone with High Productivity, Salix Pet-Susu Clone KKD. *J. Jpn. Inst. Energy* **2012**, *91*, 948–953. [CrossRef]
32. Hanaoka, T.; Sakanishi, K.; Okumura, Y. The Effect of $N_2/CO_2/O_2$ Content and Pressure on Characteristics and CO_2 Gasification Behavior of Biomass-Derived Char. *Fuel Process. Technol.* **2012**, *104*, 287–294. [CrossRef]
33. Koido, K.; Hoshi, T.; Sato, M. Hardwood Branch Char Gasification with CO_2: Characterization of Reactivity and Proposal of a Semiempirical Kinetic Model. *Energy Fuels* **2023**, *37*, 17359–17372. [CrossRef]
34. Bhatia, S.K.; Perlmutter, D.D. A Random Pore Model for Fluid-Solid Reactions: I. Isothermal, Kinetic Control. *AIChE J.* **1980**, *26*, 379–386. [CrossRef]
35. Okumura, Y.; Hanaoka, T.; Sakanishi, K. Enhancement of Gasification Rate of Biochar under Low-Temperature Conditions by Directly Supported Catalysts. *Trans. JAPAN Soc. Mech. Eng. Ser. B* **2013**, *79*, 2798–2809. [CrossRef]
36. Sato, R.; Kadoma, T.; Fujimoto, Y.; Ogata, N.; Yabuuchi, K.; Ninomiya, Y.; Horio, M. Effect of Aluminum Oxide Additives for Suppressing Clinker Formation in a Co-Current Up-Flowing Moving Bed Gasifier Fueled by Japanese Cedar Pellets. *J. Jpn. Inst. Energy* **2021**, *100*, 245–253. [CrossRef]